

Exciton spin relaxation in quantum dots measured using ultrafast transient polarization grating spectroscopy

Gregory D. Scholes,* Jeongho Kim, and Cathy Y. Wong

*Lash-Miller Chemical Laboratories, 80 St. George Street, Centre for Quantum Information and Quantum Control,
and Institute for Optical Sciences, University of Toronto, Toronto, Ontario, Canada M5S 3H6*

(Received 13 February 2006; published 24 May 2006)

On the basis of quantum dot exciton states and selection rules for their excitation, a microscopic picture of a nonlinear optical spectroscopy that provides a direct probe of spin relaxation among quantum dot exciton states is described. Equations of motion which govern the evolution of the third order exciton population density are solved numerically to simulate the measured signals. It is shown how cross linearly-polarized pulse sequences in three-pulse transient grating experiments form a polarization grating that monitors the history of the bright exciton ($F=\pm 1$) spin states. Spin flips among those states lead to a decay of the grating, and consequently the diffracted probe signal. In the microscopic picture elucidated from the simulations, destructive interference between the third-order polarizations radiated by populations of excitons with flipped and conserved spin states causes the signal decay. The experiment permits the direct observation of the kinetics of exciton spin state flips in an isotropic ensemble of quantum dots. Such measurements are demonstrated for colloidal CdSe quantum dots at room temperature, and compared with results for a control experiment. The relationship between this experiment and a difference measurement based on circularly-polarized pump and probe pulses is established.

DOI: [10.1103/PhysRevB.73.195325](https://doi.org/10.1103/PhysRevB.73.195325)

PACS number(s): 78.47.+p, 78.67.-n, 78.67.Bf, 78.67.Hc

I. INTRODUCTION

The prospect of employing quantum spin states as a means of conveying, manipulating, or encrypting information has inspired recent advances in spintronics and quantum computation.¹⁻¹⁷ Quantum dots (QDs) are envisioned as key component materials for such technologies owing to their well defined electronic states.¹⁸⁻²³ One means of establishing a spin population is to use optical pumping, whereby the photon angular momentum of circularly polarized light is transferred to excitons in a semiconductor.²⁴⁻²⁸ There has been a resurgence of interest in such optical orientation,²⁹⁻³⁴ in particular its application to QDs,³⁵⁻⁴⁰ owing to applications for the study and implementation of schemes for quantum computation. In the present work we describe a means for measuring ultrafast exciton spin relaxation in an ensemble of randomly oriented quantum dots.

QD spectroscopy is described in terms of single-excitation configurations mapping the possible ways that an electron can be promoted from the fourfold degenerate valence band to the doubly-degenerate conduction band.⁴¹⁻⁴³ Those configurations are mixed by the exchange interaction, leading to an exciton fine structure.⁴³⁻⁶⁴ The fine structure manifold spans approximately 40 meV for small colloidal QDs and is therefore obscured in frequency domain ensemble spectroscopies by inhomogeneous line broadening. Evidence for the existence of the exciton fine structure comes from careful photoluminescence studies of ensembles and single QDs.^{44,65-68} It has been proposed that these fine structure states can be further mixed by the nonanalytic, or long-range, exchange interaction.^{58,62,69,70} In that case the lowest dark excitons are perturbed little, but the lowest bright excitons mix, removing their degeneracy and changing the selection rules for their excitation. At higher tempera-

tures, rather than a splitting in the frequency domain, the perturbation attributed to the long-range exchange may flip the spin from one bright exciton state to another. In other words, the total angular momentum of an exciton state may flip from $F=+1$ to $F=-1$ and *vice versa* subsequent to photoexcitation. The time scale of those dynamics determines the relaxation time of exciton spin states in QDs.

In recent work an ultrafast coherent spectroscopy was proposed that could, in principle, monitor the dynamics of spin relaxation among $F=\pm 1$ excitons in ensembles of randomly oriented QDs.⁷¹ Despite the degeneracy of those exciton states, the dynamics can be probed through a change in sign of the radiated third-order polarization, thus providing a means of keeping track of the *history* of the QD exciton. That is, whether the exciton state being probed has the same total angular momentum as that initially photoexcited. As such, optical orientation of the exciton states is unnecessary for the success of the experiment. Subsequently we applied the method to examine the size dependence of exciton spin relaxation in CdSe QDs.⁷² In that work we discovered that the rate of spin relaxation is strongly size dependent, ranging from <100 fs to 1.2 ps for samples with mean diameters ranging from 3.1 nm to 5.0 nm. The way that the polarization grating 3-TG experiment works is nonintuitive because it is a coherent nonlinear process. Furthermore, the necessary consideration of selection rules, particularly those for QD excitons, in the nonlinear response formalism for orientationally isotropic ensembles is new. The aim of the present report is to clarify aspects of the polarization grating 3-TG experiment by providing a detailed examination of the method, QD selection rules and their orientation dependence, and an experimental verification of the theory.

The organization of the paper is as follows. In the next section we describe the exciton states, selection rules, and

the principle of optical orientation for QDs. That establishes the essential background for for the remainder of the paper, which is concerned with the measurement of exciton spin relaxation among the quantum dot bright exciton states that have total angular momentum $F = \pm 1$. The spin relaxation detected in the experiments described in this contribution is caused by flipping among those bright exciton states. Relaxation to the dark states does not contribute to the signal decay. In Sec. III the linear cross-polarized third-order transient grating (3-TG), or transient polarization grating, experiment is described and signals are simulated by solving the equations of motion that dictate the temporal evolution of the third-order density matrix. Thus a microscopic picture of precisely how the polarization grating 3-TG experiment measures spin relaxation is presented. Importantly, the theory has been derived to model experiments on ensembles of colloidal quantum dots, where each QD in the ensemble is oriented randomly relative to the laboratory frame. Significant rotational diffusion does not occur on the time scale of the measurements described in this work. In Sec. IV we describe the experimental setup, then in Sec. V the results of experiments that demonstrate and test the theory are reported. In Sec. VI we discuss the interpretation of optical orientation by circularly polarized light of excitons in isotropic quantum dot ensembles. It is shown that information equivalent to the linear crossed polarized 3-TG experiment can be obtained as a difference measurement between two pulse sequences with permutations of circular polarizations. That result provides an alternative picture for understanding the measurement of spin relaxation, providing a closer connection to established concepts of optical orientation. In the Appendixes the orientation dependence of QD absorption is examined and the conclusion that optical orientation is reversed when the QD is oppositely-facing relative to the propagation of the incident light is derived and justified.

II. OPTICAL EXCITATION OF QUANTUM DOTS

The valence and conduction band states of semiconductors are characterized according to their total angular momentum and its projection onto the positive z axis, m_j . In typical binary semiconductors with zinc blende or wurtzite structures, the z axis has a particular orientation because those crystals lack inversion symmetry.⁷³ Ignoring exchange interactions for the moment, excitons with total angular momentum $F = \pm 1$ can be prepared by photoexciting a valence band electron to the conduction band using circularly-polarized light, as indicated in Fig. 1. That idea underpins *optical orientation*, whereby a majority of a specified spin state can be established by photoexcitation of a suitably oriented semiconductor crystal with respect to the propagation direction of the incident circularly-polarized (CP) light.^{24–26} That is because CP light with momentum \mathbf{k} has an angular momentum component $\pm\hbar$ along \mathbf{k} according to whether it is right- or left-CP respectively. The spatial distribution of the electric field vector of CP light maps a right spiral onto the (x, y, z) coordinate system,⁷⁴ thus

$$\sigma^{(+)} = \hat{e}_R = (\hat{e}_x + i\hat{e}_y)/\sqrt{2}, \quad (1a)$$

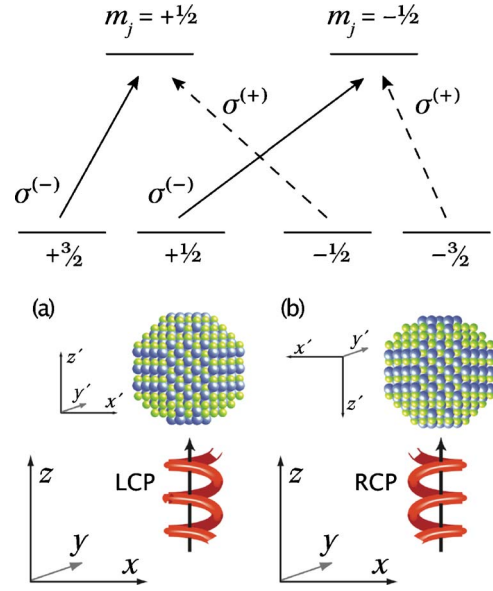


FIG. 1. (Color online) Upper panel: The valence and conduction band states of a prototypical semiconductor are characterized according to the projection of the total angular momentum onto the positive z axis, m_j . Solid lines depict valence to conduction band excitations of an electron that are promoted by absorption of left-hand circularly polarized light [$\sigma^{(-)} = \hat{e}_L = (\hat{e}_x - i\hat{e}_y)/\sqrt{2}$], while dashed lines indicate the absorption of right-hand circularly polarized light [$\sigma^{(+)} = \hat{e}_R = (\hat{e}_x + i\hat{e}_y)/\sqrt{2}$]. Lower panel: Two relative orientations of the QD local reference frame (x', y', z') relative to the fixed (laboratory) axis system (x, y, z) are shown. In each case the incoming photon propagates along \hat{z} . Considering the selection rules for one-photon absorption, it can be shown that in (a) left-hand circularly polarized light excites the Ψ_{-1} QD exciton. However, when the QD is rotated 180° right-hand circularly polarized light excites that same exciton.

$$\sigma^{(-)} = \hat{e}_L = (\hat{e}_x - i\hat{e}_y)/\sqrt{2}, \quad (1b)$$

where the \hat{e}_λ are polarization unit vectors of right-hand (RH) and left-hand (LH) CP light, $\lambda = R, L$, or light that is linearly polarized in the plane normal to the propagation direction, $\lambda = x, y$. There is inconsistency in the literature regarding the labeling of $\sigma^{(+)}$ and $\sigma^{(-)}$ as RH or LH CP light. Here the definition of Jones⁷⁵ is used.

The principle of optical orientation may also be applied to suitably oriented semiconductor quantum dots (QDs). Since the exchange interaction is significant in magnitude for small QDs relative to the bulk, its influence on the mixing between single-excitation configurations needs to be considered.⁷⁶ The single-excitation configurations are written as products of electron and hole wave functions⁴³

$$\psi_{\alpha, M}(\mathbf{r}_e, \mathbf{r}_h) = \phi_\alpha(\mathbf{r}_e) \phi_M(\mathbf{r}_h). \quad (2)$$

The electron and hole wave functions are each written as the product of an envelope function $\xi(\mathbf{r})$ and a Bloch function^{41–43,77}

$$\phi_\alpha(\mathbf{r}_e) = \xi(\mathbf{r}_e) |S\alpha\rangle, \quad (3)$$

$$\phi_M(\mathbf{r}_h) = \sum \xi'_\mu(\mathbf{r}_h) u_\mu, \quad (4)$$

where u_μ , with $\mu = \pm\frac{1}{2}, \pm\frac{3}{2}$, are Bloch functions of the valence band at Γ_8 , written according to the Luttinger-Kohn convention as

$$u_{3/2} = \frac{1}{\sqrt{2}}(X + iY)\uparrow, \quad (5a)$$

$$u_{-3/2} = \frac{i}{\sqrt{2}}(X - iY)\downarrow, \quad (5b)$$

$$u_{1/2} = \frac{i}{\sqrt{6}}[(X + iY)\downarrow - 2Z\uparrow], \quad (5c)$$

$$u_{-1/2} = \frac{1}{\sqrt{6}}[(X - iY)\uparrow + 2Z\downarrow]. \quad (5d)$$

In the present work we are concerned with electric-dipole transition matrix elements for excitation of excitons in QDs. They are obtained as a product of an overlap integral over the slowly-varying envelope functions, $K' \equiv \sqrt{K}$, with a matrix element between Bloch functions.⁴¹ The angular integral over the product of spherical harmonics $\int d\Omega Y_{lm} Y_{00} = \delta_{l0}$ that contributes to K' simplifies the hole wave functions. Then the electric-dipole transition matrix element for one-photon absorption from valence band to conduction band in the electron-electron representation is

$$\boldsymbol{\mu}_{M,\alpha} = \langle \phi_\alpha | -e\mathbf{r} | \phi_M \rangle = K' \langle S\alpha | \hat{\boldsymbol{\mu}} | u_{\mu=M} \rangle. \quad (6)$$

The states $\psi_{\alpha,M}$ are mixed by the short-range exchange interaction to form the manifold of QD exciton states Ψ_F with total angular momentum $F = s_z + M$ and energies that form the QD exciton fine structure

$$\Psi_{+2} = \psi_{\uparrow,3/2}, \quad (7a)$$

$$\Psi_{-2} = \psi_{\downarrow,-3/2}, \quad (7b)$$

$$\Psi_{+1}^L = iC^+ \psi_{\uparrow,1/2} + C^- \psi_{\downarrow,3/2}, \quad (7c)$$

$$\Psi_{-1}^L = iC^- \psi_{\uparrow,-3/2} + C^+ \psi_{\downarrow,-1/2}, \quad (7d)$$

$$\Psi_0^L = [i\psi_{\uparrow,-1/2} + \psi_{\downarrow,1/2}]/\sqrt{2}, \quad (7e)$$

$$\Psi_{+1}^U = -iC^+ \psi_{\uparrow,1/2} + C^- \psi_{\downarrow,3/2}, \quad (7f)$$

$$\Psi_{-1}^U = -iC^- \psi_{\uparrow,-3/2} + C^+ \psi_{\downarrow,-1/2}, \quad (7g)$$

$$\Psi_0^U = [-i\psi_{\uparrow,-1/2} + \psi_{\downarrow,1/2}]/\sqrt{2}, \quad (7h)$$

where C^\pm are mixing coefficients defined by Efros *et al.*⁴³ The electric dipole transition moment vectors for excitation of each of these exciton states $|\zeta\rangle$ from the ground state $|0\rangle$, $\boldsymbol{\mu}^{\zeta 0} \equiv \boldsymbol{\mu}^\zeta$, are

$$\boldsymbol{\mu}^{\pm 2} = 0, \quad (8a)$$

$$\boldsymbol{\mu}^{\pm 1(L)} = \frac{C^+ K' \sqrt{2} + C^- K' \sqrt{6}}{2\sqrt{3}} (\vec{\mu}_x \mp i\vec{\mu}_y), \quad (8b)$$

$$\boldsymbol{\mu}^{0(L)} = 0, \quad (8c)$$

$$\boldsymbol{\mu}^{\pm 1(U)} = \frac{\mp C^+ K' \sqrt{2} \pm C^- K' \sqrt{6}}{2\sqrt{3}} (\vec{\mu}_x \mp i\vec{\mu}_y), \quad (8d)$$

$$\boldsymbol{\mu}^{0(U)} = -i \frac{K'}{\sqrt{3}} \vec{\mu}_z. \quad (8e)$$

The matrix element for one-photon absorption from the QD ground state $|0\rangle$ to the exciton state $|\zeta\rangle$ in the electric dipole approximation is⁷⁸

$$M_{\zeta 0} = \langle \zeta | (n-1)(\mathbf{k}, \lambda) | -\epsilon_0^{-1} \boldsymbol{\mu} \cdot \mathbf{d}^\perp(\mathbf{R}) | n(\mathbf{k}, \lambda) | 0 \rangle, \quad (9)$$

where $n(\mathbf{k}, \lambda)$ is the occupation number for the quantized radiation field for photons of wave vector \mathbf{k} and polarization λ . The QD is located at \mathbf{R} . That expression is evaluated using the mode expansion for the transverse displacement vector

$$\mathbf{d}^\perp(\mathbf{r}) = i \sum_{\mathbf{k}, \lambda} \left(\frac{\hbar c k \epsilon_0}{2V} \right)^{1/2} [\mathbf{e}^{(\lambda)}(\mathbf{k}) a^{(\lambda)}(\mathbf{k}) e^{i\mathbf{k} \cdot \mathbf{r}} - \bar{\mathbf{e}}^{(\lambda)}(\mathbf{k}) a^{\dagger(\lambda)}(\mathbf{k}) e^{-i\mathbf{k} \cdot \mathbf{r}}], \quad (10)$$

where V is the quantization volume, $\mathbf{e}^{(\lambda)}(\mathbf{k})$ denotes the photon polarization, a and a^\dagger are annihilation and creation operators for the radiation field, and the bar indicates complex conjugate. The matrix element for absorption is therefore

$$M_{\zeta 0} = -i \left(\frac{\hbar c k}{2\epsilon_0 V} \right)^{1/2} \mathbf{e}^{(\lambda)}(\mathbf{k}) \cdot \boldsymbol{\mu}^{\zeta 0} e^{i\mathbf{k} \cdot \mathbf{R}}. \quad (11)$$

The absorption probability depends on $|M_{\zeta 0}|^2$. Similarly we can evaluate the matrix element for one-photon emission, obtaining

$$M_{0\zeta} = i \left(\frac{\hbar c k}{2\epsilon_0 V} \right)^{1/2} \bar{\mathbf{e}}_j^{(\lambda)}(\mathbf{k}) \cdot \boldsymbol{\mu}_j^{0\zeta} e^{-i\mathbf{k} \cdot \mathbf{R}}, \quad (12)$$

where it is necessary to sum over all possible photon directions and polarizations (hence the index j) in a solid angle relevant to the detection direction. Note that $\boldsymbol{\mu}^{0\zeta}$ equals the complex conjugate of $\boldsymbol{\mu}^{\zeta 0}$ [i.e. $(\boldsymbol{\mu}^{\zeta 0})^*$].

Considering Eqs. (8) in conjunction with Eq. (11) it is deduced that $\Psi_{+1}^{U,L}$ are exclusively photoexcited by RH CP light ($\sigma^{(+)}$) propagating along the QD z direction, while $\Psi_{-1}^{U,L}$ states are excited by LH CP light ($\sigma^{(-)}$). Light that is linearly polarized in the (x,y) plane may excite any of the $\Psi_{\pm 1}^{U,L}$ states.

III. TRANSIENT POLARIZATION GRATINGS AND QUANTUM DOT EXCITON SPIN RELAXATION

Many spectroscopic investigations of QDs are undertaken for colloidal samples, which are typically randomly oriented. In such samples the exciton fine structure is obscured by inhomogeneous line broadening, so individual states cannot

be selected by tuning the frequency of the excitation light. Polarized excitation light may allow one to probe the fine structure exciton states with greater selectivity. In that case, resonant nonlinear optical spectroscopy has great potential; the higher the order of the spectroscopy, the more diverse the opportunities for using polarization to gather information from an isotropic ensemble.^{71,79–83} On that basis an analysis of polarization sequences for various resonant third-order nonlinear spectroscopies and their application to QDs was reported.⁷¹ It was found that cross-linear polarized pulses could be used to detect exciton spin relaxation among the $F=\pm 1$ exciton states. That idea is scrutinized more closely in this section.

In third-order resonant transient grating (3-TG) spectroscopy two time-coincident laser pulses with wave vectors \mathbf{k}_1 and \mathbf{k}_2 are crossed at a small angle θ in a medium.^{84,85} We use an angle $\theta \approx 2.2^\circ$, which means that the beams can be treated as approximately colinear for the purposes of the microscopic theory described below. Interference between these two laser beams at their crossing point in the sample creates a population grating—a sinusoidal modulation of the probability of finding QD excitons. A variably delayed probe pulse with wave vector \mathbf{k}_3 interrogates the temporal evolution of the QD excitons via the time-integrated intensity $I(t_p)$ of an induced third-order polarization $\mathbf{P}^{(3)}(0, t_p, t)$ scattered in the $\mathbf{k}_s = -\mathbf{k}_1 + \mathbf{k}_2 + \mathbf{k}_3$ signal direction. The time variables correspond to the delay among the pump pulse pair, set to zero, the delay between those pulses and the probe, t_p , and the subsequent time evolution of the radiated polarization over t . The experimental detection scheme integrates over t . The experiments described here detect phenomena that occur on a time-scale orders of magnitude faster than decay of the grating caused by spatial diffusion processes. Thus only dynamics intrinsic to the QDs are probed.

Two basic varieties of 3-TG experiment are possible, as determined by the polarization configuration of the pump pulses. These are known as intensity (or population) grating and polarization grating experiments. In an intensity grating experiment the intensity of the induced polarization radiated in the \mathbf{k}_s direction depends on the modulation depth. The signal therefore decays as the excitons recombine, thereby revealing much that same kind of information as a pump probe experiment. The polarization sequence of the pump pair, electric fields $\mathbf{E}_1, \mathbf{E}_2$, probe \mathbf{E}_3 , and signal \mathbf{E}_4 is written as $\hat{e}_1 \hat{e}_2 \hat{e}_3 \hat{e}_4$. Intensity grating experiments then include 3-TG experiments carried out using the polarization sequences RRRR, LLLL, RRLL, VVVV, RRVV, and VVHH, where R means RH CP light and L means LH CP light [Eq. (1)], V denotes linear vertically-polarization light ($\hat{e}_V = \hat{e}_x$), and H is horizontally-polarized light ($\hat{e}_H = \hat{e}_y$). The light is propagating in the z direction.

When the pump pulses are orthogonally polarized, that is $\hat{e}_1 \cdot \hat{e}_2 = 0$, then a polarization grating is formed in the sample. In that case there is no spatially-modulated intensity grating, but QDs in the beam crossing volume may be photoexcited. The distinguishing feature of this experiment is that the polarization of the grating varies spatially according to the phase delay between \mathbf{E}_1 and \mathbf{E}_2 . A suitably polarized probe beam can detect the decay of this polarization, which might

be instigated by phenomena such as rotational diffusion, resonance energy transfer, and so on. That can be understood in the context of the grating decomposition method proposed by Fourkas *et al.*⁸⁶ Polarization sequences for this experiment include VHVH, VHHV, RLRL. Sequences such as VHVV yield zero signal, as is obvious from inspection of the row vector in Eq. (B5).

A characteristic of the crossed-linear polarization grating is that the spatial polarization modulation spans LH CP to RH CP via elliptical and linear polarization.⁸⁷ Such an intuitive understanding of polarization and population gratings has enabled the method to be applied to a diverse range of systems.^{84–95} Hence one might surmise that the origin of the signal decay when the experiment is applied to quantum dots relates to the selection rules for exciton photoexcitation and the circular-polarization character of the grating. However, it does not seem that the VHVH and VHHV experiments for QDs can be easily comprehended by considering the pump pulse sequence in isolation from the probe/analyzer. Actually, that conclusion is generally true for coherent nonlinear spectroscopies.^{96,97} To comprehend the relationship between the VHVH and VHHV 3-TG experiments and the QD exciton states it must be realized that the populations of Ψ_{+1} and Ψ_{-1} excitons are equal and contiguous across the grating, despite the polarization modulation. Recall that those exciton states cannot be oriented in an isotropic ensemble. The experiment can best be understood by considering the full third-order response, and it thus emerges that the manner by which the grating is probed is crucial. This will be shown here through simulations of the experiment.

The heterodyne-detected and homodyne 3-TG signal intensities as a function of probe delay t_p are given by

$$I_{HET}(t_p) \propto \int_0^\infty dt \operatorname{Re}[\mathbf{E}_{LO}^*(t_p, \Delta\phi) \cdot \langle \mathbf{P}^{(3)}(0, t_p, t) \rangle], \quad (13a)$$

$$I_{HOM}(t_p) \propto \int_0^\infty dt |\langle \mathbf{P}^{(3)}(0, t_p, t) \rangle|^2, \quad (13b)$$

where $\Delta\phi$ is the phase delay between the local oscillator field \mathbf{E}_{LO}^* and the probe field \mathbf{E}_3 . The angle brackets indicate a rotational average. The electric field of the laser pulse j has the form

$$\mathbf{E}_j(\omega, t) = \hat{e}_j A(t) \cos(\omega_0 t), \quad (14)$$

where ω_0 is the carrier frequency, \hat{e}_j is the polarization and $A(t) = \exp[-4 \ln 2 t^2 / \tau_E^2]$ is the pulse envelope. At low excitation intensities the third-order polarization radiated by the sample is determined by a perturbation expansion of the density matrix ρ to third-order in the field-matter interactions⁹⁶

$$\mathbf{P}^{(3)}(0, t_p, t) = \operatorname{Tr}(N \boldsymbol{\mu} \cdot \rho^{(3)}). \quad (15)$$

Here a model system is considered in order to communicate the cross-polarized 3-TG experiment for probing QD exciton spin relaxation. To that end, a ground state $|0\rangle \equiv |g\rangle$ and two excited states corresponding to the $F=\pm 1$ exciton states $|\Psi_{+1}\rangle \equiv |p\rangle$ and $|\Psi_{-1}\rangle \equiv |m\rangle$ are considered, Fig. 2.

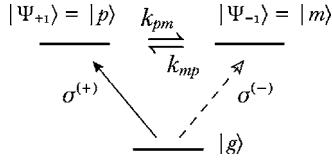


FIG. 2. Kinetic scheme used for simulations of the 3-TG signals. The exciton states interconvert according to the rate constants k_{pm} and k_{mp} .

Spin flips between the QD $|p\rangle$ and $|m\rangle$ states may occur with a rate k_s . More specifically, the $|p\rangle$ to $|m\rangle$ spin relaxation rate is designated to be k_{pm} and the reverse rate to be k_{mp} . To keep track of the selection rules applying to excitation of the exciton versus those for probing the final state, a population that has flipped from its original exciton state is designated by a dash. For example, $|m'\rangle$ means $|\Psi_{-1}\rangle$ population at some time after the pump sequence that was originally photoexcited to the $|p\rangle$ state.

The time-ordered sequence of incident laser pulses is $\mathbf{E}_1(-t_p)$, $\mathbf{E}_2(-t_p)$, and $\mathbf{E}_3(0)$. An analyzer exerts the final polarization control on the radiated signal via \hat{e}_4 . The calculated signal includes equal contributions from pulse time orderings 1-2-3 and 2-1-3, since the pump pulses are temporally overlapped. To simplify the presentation, just the normal time ordering and one representative rephasing pathway is described here explicitly.

At any time after the pump sequence, two reservoirs of each of the $|p\rangle$ and $|m\rangle$ exciton population densities are considered: those that have the same spin as originally prepared by the optical excitation, $\rho_{pp} = |p\rangle\langle p|$ and $\rho_{mm} = |m\rangle\langle m|$, and those excitons that are in an opposite spin state to that originally prepared, $\rho_{p'p'}$ and $\rho_{m'm'}$. It is important to keep track of the QD transition moments, which of course change after a spin flip during the delay t_p over which the exciton populations evolve. A simplified way of envisioning the consequences of that spin flip is to imagine that the final incident field “sees” an opposite transition moment to that which enabled absorption of the incident light.

The contribution to the density matrix at third-order with respect to radiation-matter interactions $\rho^{(3)}$ is obtained by solving coupled differential equations that describe how the material system interacts with the incident electromagnetic field, thus obtaining the induced third-order polarization of Eq. (15). A more detailed description of this well-known theory can be found in Refs. 96 and 97. Thus $\rho^{(3)}$ is calculated by solving the following coupled differential equations (and four others where $p \rightarrow m$):

$$\frac{\partial}{\partial t} \rho_{gp}^{(1)} = \frac{i}{\hbar} [\epsilon_{pg}^* E_1 \rho_{gg}^{(0)} + \epsilon_p \rho_{gp}^{(1)}] - \gamma \rho_{gp}^{(1)}, \quad (16a)$$

$$\frac{\partial}{\partial t} \rho_{pp}^{(2)} = -\frac{i}{\hbar} \epsilon_{pg}^2 E_2 \rho_{gp}^{(1)} - k_{pm'} \rho_{pp}^{(2)} + k_{m'p} \rho_{m'm'}^{(2)} - \Gamma \rho_{pp}^{(2)}, \quad (16b)$$

$$\frac{\partial}{\partial t} \rho_{m'm'}^{(2)} = k_{pm'} \rho_{pp}^{(2)} - k_{m'p} \rho_{m'm'}^{(2)} - \Gamma \rho_{m'm'}^{(2)}, \quad (16c)$$

$$\frac{\partial}{\partial t} \rho_{gg}^{(2)} = \frac{i}{\hbar} [\epsilon_{gp}^2 E_2 \rho_{gp}^{(1)} + \epsilon_{gm}^2 E_2 \rho_{gm}^{(1)}] + \Gamma [\rho_{pp}^{(2)} + \rho_{m'm'}^{(2)} + \rho_{mm}^{(2)} + \rho_{p'p'}^{(2)}], \quad (16d)$$

$$\frac{\partial}{\partial t} \rho_{pg}^{(3)} = \frac{i}{\hbar} [\epsilon_{gp}^3 E_3 \rho_{pp}^{(2)} + \epsilon_p \rho_{pg}^{(3)}] - \gamma \rho_{pg}^{(3)}, \quad (16e)$$

where $\epsilon_p = \epsilon_m$ are the transition energies for excitation of $|p\rangle$ and $|m\rangle$, γ is the dephasing time of a coherence, Γ is the decay time of the exciton states, $E_j = A(t) \cos(\omega_0 t)$ and the couplings between the incident polarizations and the QD transition moments are written as

$$\epsilon_{ji}^n = \langle j | -\mathbf{e}_n \cdot \boldsymbol{\mu} | i \rangle, \quad (17a)$$

$$\epsilon_{ji}^{n*} = \langle i | -\mathbf{e}_n^* \cdot \boldsymbol{\mu} | j \rangle, \quad (17b)$$

as is discerned from M_{i0} in Eq. (11). These terms need to be collected and rotationally averaged, as shown below in Eq. (18).

According to the factorization approximation,⁹⁸ Eq. (15) together with Eqs. (16) yield the macroscopic polarization radiated by the sample in the $\mathbf{k}_s = -\mathbf{k}_1 + \mathbf{k}_2 + \mathbf{k}_3$ phase-matched direction

$$\begin{aligned} \mathbf{P}^{(3)}(0, t_p, t) &= \langle \epsilon_{pg}^1 \epsilon_{pg}^2 \epsilon_{gp}^3 \epsilon_{gp}^{4*} \rangle \rho_1^{(3)}(0, t_p, t) + \langle \epsilon_{pg}^1 \epsilon_{pg}^2 \epsilon_{gm'}^3 \epsilon_{gm'}^{4*} \rangle \rho_2^{(3)} \\ &\quad \times (0, t_p, t) + \langle \epsilon_{mg}^1 \epsilon_{mg}^2 \epsilon_{gm}^3 \epsilon_{gm}^{4*} \rangle \rho_3^{(3)}(0, t_p, t) \\ &\quad + \langle \epsilon_{mg}^1 \epsilon_{mg}^2 \epsilon_{gp'}^3 \epsilon_{gp'}^{4*} \rangle \rho_4^{(3)}(0, t_p, t) \\ &= \mathbf{P}_1^{(3)}(0, t_p, t) + \mathbf{P}_2^{(3)}(0, t_p, t) + \mathbf{P}_3^{(3)}(0, t_p, t) \\ &\quad + \mathbf{P}_4^{(3)}(0, t_p, t), \end{aligned} \quad (18)$$

where the angle brackets indicate that rotational averages are to be taken over the polarization—dipole transition matrix element products and the asterisk means complex conjugate. The method for performing the tensorial rotational averaging is described in Appendix B. Using the results reported previously in Table 2 of Ref. 71, the stimulated emission contributions to the VHVH 3-TG signals result from

$$\mathbf{P}_1^{(3)}(0, t_p, t) = \frac{2}{15} |\boldsymbol{\mu}_{pg}|^4 \rho_1^{(3)}(0, t_p, t), \quad (20a)$$

$$\mathbf{P}_2^{(3)}(0, t_p, t) = -\frac{2}{15} |\boldsymbol{\mu}_{pg}|^2 |\boldsymbol{\mu}_{mg}|^2 \rho_2^{(3)}(0, t_p, t), \quad (20b)$$

$$\mathbf{P}_3^{(3)}(0, t_p, t) = \frac{2}{15} |\boldsymbol{\mu}_{mg}|^4 \rho_3^{(3)}(0, t_p, t), \quad (20c)$$

$$\mathbf{P}_4^{(3)}(0, t_p, t) = -\frac{2}{15} |\boldsymbol{\mu}_{mg}|^2 |\boldsymbol{\mu}_{pg}|^2 \rho_4^{(3)}(0, t_p, t). \quad (20d)$$

Other polarization sequences may be considered in the scheme, as has been reported previously. The coefficients $C^{(4)}$ relevant to Eqs. (20), were reported in Ref. 71 and are collected here in Table 1 of Appendix B.

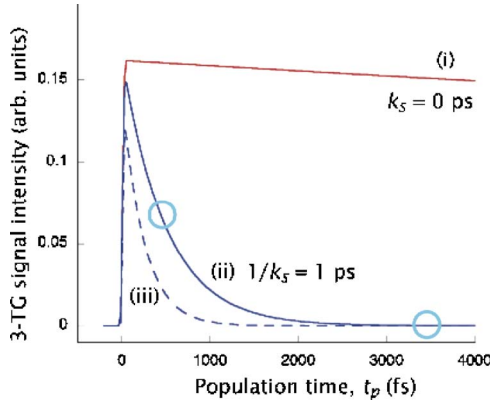


FIG. 3. (Color online) Calculated imaginary (absorptive) contribution to the heterodyne-detected VHVH 3-TG signals for cases of (i) no spin flips, where the decay of the signal follows exciton population recombination, and (ii) a spin flip time $1/k_s$ of 1 ps. The dashed line (iii) shows the homodyne-detected signal calculated for the same conditions as (ii).

In Fig. 3 calculated VHVH 3-TG signals are shown. Curve (i) represents a model heterodyne-detected signal in the absence of spin flip transitions ($k_s=0$). The population relaxation time Γ is arbitrarily set to 50 ps for the purposes of the present model simulations. That decay time is evident as the decaying component of the simulated 3-TG curve (i) since the signal intensity is proportional to the exciton population density $\rho_{pp} + \rho_{mm}$. Curve (ii) shows the imaginary component of the heterodyne-detected 3-TG signal calculated with $k_{pm}=k_{mp}=k_s=1 \text{ ps}^{-1}$. The markedly different decay is

evident, and is clearly dictated by a relaxation rate $2k_s$ rather than Γ . Curve (iii) shows the corresponding homodyne signal, which decays twice as fast as (ii) owing to the modulus squared in Eq. (13b).

To understand the origin of the 3-TG signal decay as a function of delay time t_p it is helpful to isolate individual pathways contributing to $\mathbf{P}^{(3)}(0, t_p, t)$ in Eq. (19). In Fig. 4(a) we show each of $\mathbf{P}_1^{(3)}(0, t_p, t)$ to $\mathbf{P}_4^{(3)}(0, t_p, t)$ at $t_p=500 \text{ fs}$, plotted versus t to show the time evolving field. At this delay time (500 fs) the total 3-TG signal intensity in Fig. 3 [curve (ii)] still has a substantial magnitude. By comparing these radiated polarizations with those calculated for $t_p=3.5 \text{ ps}$, shown in Fig. 4(b), when the total time-integrated VHVH 3-TG signal in Fig. 3 has decayed to a negligible intensity, it becomes apparent that the decay of the VHVH 3-TG signal does not correspond to diminishing radiated polarizations from sources in the ensemble that reflect population relaxation. Instead, the 3-TG signal decay is actually caused by destructive interference of the $\mathbf{P}_1^{(3)}(0, t_p, t)$ and $\mathbf{P}_3^{(3)}(0, t_p, t)$ polarizations with $\mathbf{P}_2^{(3)}(0, t_p, t)$ and $\mathbf{P}_4^{(3)}(0, t_p, t)$. The reason for this is that the exciton spin flip is associated with a sign change in $C^{(4)}$ [see Eq. (B5)], and that sign change is manifest as a π phase shift of those latter two induced polarizations compared to $\mathbf{P}_1^{(3)}(0, t_p, t)$ and $\mathbf{P}_3^{(3)}(0, t_p, t)$.

Several VHVH 3-TG simulations are compared in Fig. 5. It is clear that the decay of the signal is directly related to the spin flip dynamics, consistent with our recent experimental results. Comparison of the 3-TG signal (iv) in Fig. 5(a) with the time evolution of the population densities plotted in Fig. 5(b) shows that the 3-TG signal decay is related to the population difference $(\rho_{pp} + \rho_{mm}) - (\rho_{m'm'} + \rho_{p'p'})$. Hence the kinet-

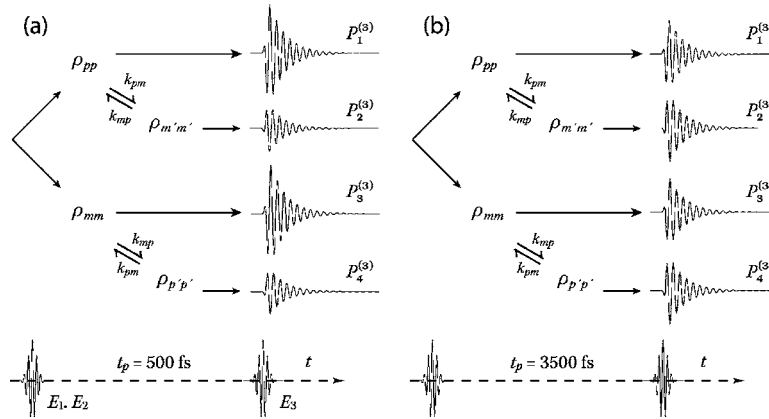


FIG. 4. Synopsis of the generation of a 3-TG signal for the VHVH experiment, showing the signal evolution for two population times. The initial pump pulse sequence (VH) creates equal numbers of $F=+1$ and $F=-1$ excitons, with corresponding densities ρ_{pp} and ρ_{mm} , respectively. If those population densities are probed at some time delay t_p later, then the corresponding third-order polarizations $P_1^{(3)}$ and $P_3^{(3)}$ are induced and radiate from the sample to be detected as a signal. That signal intensity decays with t_p according to the usual kinetics of exciton trapping and recombination. Exciton spin flips are monitored by the population densities $\rho_{m'm'}$ and $\rho_{p'p'}$. The state m' is physically indistinguishable from m , but is differentiated because while m was directly excited by the pump sequence, m' was formed by a spin flip from the state p . The VHVH 3-TG experiment can monitor the history of the exciton populations because the third-order polarizations radiated by $\rho_{m'm'}$ and $\rho_{p'p'}$, $P_2^{(3)}$ and $P_4^{(3)}$, are phase shifted by π from $P_1^{(3)}$ and $P_3^{(3)}$. The four radiated polarizations thus interfere destructively and the total signal intensity decays according to the increasing ratio of $(\rho_{pp} + \rho_{mm})$ to $(\rho_{m'm'} + \rho_{p'p'})$. To illustrate that, the time-resolved polarizations radiated at $t_p=500 \text{ fs}$ and $t_p=3500 \text{ fs}$ are compared in (a) and (b) respectively. Those conditions correspond to the circled points on the time-integrated signal shown in Fig. 3. It is clear that even though the total time-integrated signal is zero at $t_p=3500 \text{ fs}$, the exciton populations are still significant. The total signal is zero because of interference between the the radiated polarizations $\mathbf{P}_1^{(3)}(0, t_p, t)$ to $\mathbf{P}_4^{(3)}(0, t_p, t)$.

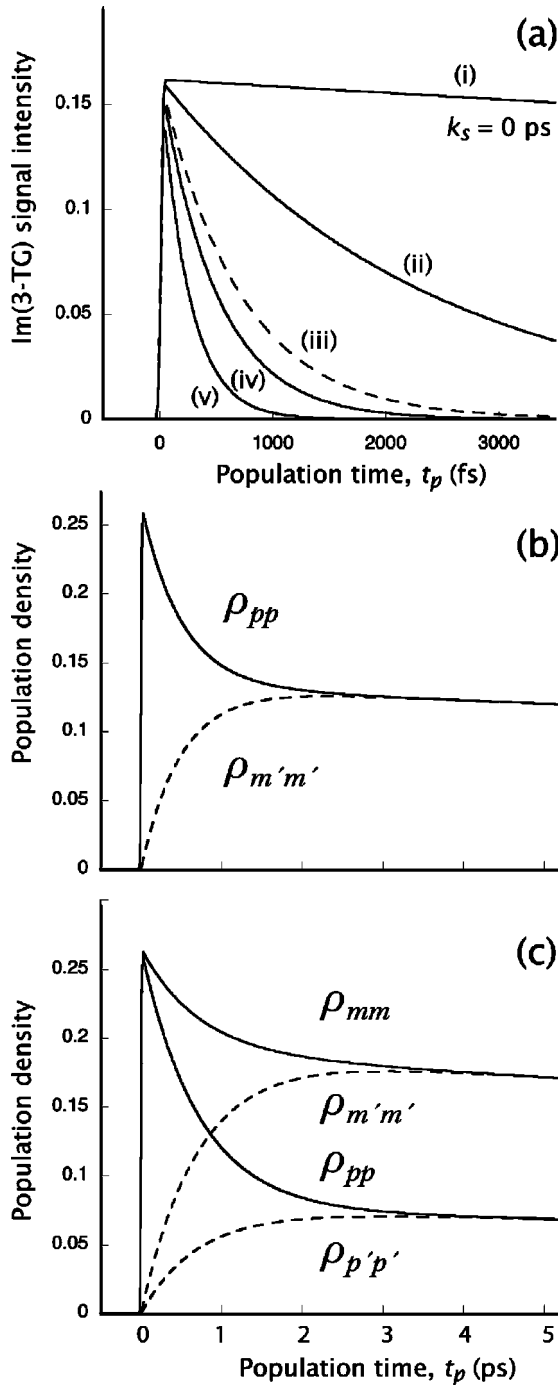


FIG. 5. (a) Simulated VHVH 3-TG decays for various spin flip rates: (i) no spin flips, (ii) $k_s^{-1}=5$ ps, (iv) $k_s^{-1}=1$ ps, (v) $k_s^{-1}=0.5$ ps. For the simulation result (iii) the forward and reverse spin flip rates differ: $k_{pm}^{-1}=1$ ps and $k_{mp}^{-1}=2.5$ ps. (b) Plot of the exciton population densities ρ_{pp} (solid line) and $\rho_{p'p'}$ (dashed line) for the simulation with $k_s^{-1}=1$ ps. (c) Similar to (b), but for simulation (iii).

ics dictating the formation of $\rho_{m'm'}$ and $\rho_{p'p'}$ via exciton spin flips dictate the VHVH 3-TG decay. It might be possible that $k_{pm} \neq k_{mp}$, for example under the influence of an applied magnetic field. According to curve (iii) in Fig. 4(a) the VHVH 3-TG signal still decays to zero amplitude once the populations shown in Fig. 4(c) equilibrate.

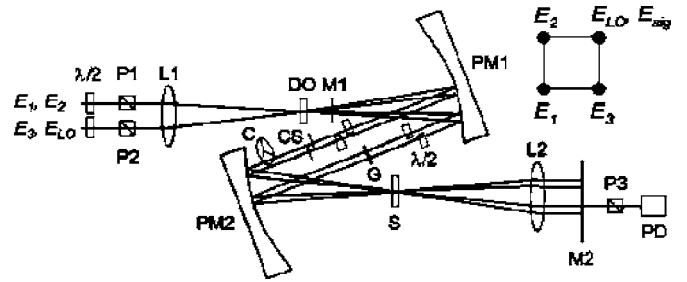


FIG. 6. Experimental setup for optical heterodyne detected transient grating (OHD-TG) measurements. $\lambda/2$: half-wave plate, P : polarizer, L : lens, DO : diffractive optics, M : PM : parabolic mirror, CS : cover slip, G : glass plate, S : sample, PD : photodiode, C : chopper.

IV. EXPERIMENTAL SECTION

Details of the laser setup have been described previously.⁹⁹ Briefly, 130 fs pulses with 800 μ J of pulse energy were generated at 775 nm from a 1 kHz-repetition rate Ti:sapphire amplified laser (Clark-MXR, CPA-2001). They were converted into visible light, tunable from 450 to 650 nm by a noncollinear optical parametric amplifier (NOPA). The NOPA output pulses were sent to a pair of quartz prisms for dispersion compensation, and then split by a beamsplitter into two beams, a strong pump, and a weak probe. A time delay between the two pulses was controlled by a motor-driven translation stage (Newport, UTM150PP.1). Both pump and probe beams separately passed through a combination of a half-wave plate and polarizer in order to control their relative intensities.

Our experimental setup of optical heterodyne detected transient grating (OHD-TG) using a diffractive optic (DO), shown in Fig. 6, is similar to those developed by Miller group¹⁰⁰ and Fleming group¹⁰¹ with a few modifications. The DO (from INO) was designed to diffract 70% of input energy into ± 1 diffractive orders. The pump and probe beams were spatially overlapped on the DO with a 10 cm focal length achromatic lens to give a pair of replicas for each pulse. The resulting four beams were achromatically collimated and focused into the sample by a pair of 10 cm focal length parabolic mirrors. Half-wave plates were inserted in order to control the polarization of each beam. To avoid any pump-probe signal contributed by the DO itself, the pump and probe beams arrive at the DO at a relative time delay shifted from t_p by 6.7 ps. A glass plate inserted into each replica of the pump beam after the DO corrects the relative time delay to t_p , simultaneously shifting the instantaneous DO pump-probe signal to $t_p = -6.7$ ps and hence shifting it out of our measurement window. To prevent any dispersion mismatch caused by insertion of the glass material in the path of the pump beam, another glass plate of the same thickness was inserted into the probe beam before the DO.

Owing to the phase matching boxcar geometry of the four incident beams, the signal field ($\mathbf{k}_s = -\mathbf{k}_1 + \mathbf{k}_2 + \mathbf{k}_3$) was radiated along the same direction as the local oscillator (\mathbf{k}_{LO}). The spatial and temporal overlap of the radiated signal field with the LO enabled the passively phase-locked optical heterodyne detection. In order to adjust accurately the phase

difference between the LO and signal fields, two identical cover slips were inserted into the probe and LO beams and one of them was adjusted by a motor-driven rotator (Thorlabs, CR1-Z6). This capability of arbitrary phase setting enables selective measurement of absorptive (imaginary) and refractive (real) components of the third-order polarization. Imaginary and real components can each be measured when the phase of LO field is set in quadrature or in phase with the signal field, respectively. To determine the phase between the two fields, the signal of a pure solvent (e.g., CS₂ or toluene) was measured while varying the relative angles between two cover slips. The nonresonant signal from pure, transparent solvent has a nearly zero absorptive contribution at visible wavelengths, so the relative phase for measuring imaginary and real components correspond to zero and maximum (or minimum) amplitude of the solvent signal, respectively. To prevent contamination from unwanted pump-probe signals induced by the LO and the pump beams, the probe beam (\mathbf{k}_3) was chopped at 250 Hz in front of the sample. To obtain the OHD-TG signal free of any homodyne signal, two signals phase shifted by π were measured, then subtracted from each other. For the measurements shown in this paper, we define the phase such that the real component of the pure solvent is positive.

The OHD-TG signal was detected using a silicon photodiode (Thorlabs, DET210) and a lock-in amplifier (Stanford Research, SR810). To ensure that only the signal and LO fields were incident on the detector, all unwanted beams and scattered light were blocked by a mask after the sample. A third polarizer was mounted after the mask to set the signal polarization. Depending on the laser center frequency, pulse durations of 30 to 40 fs were obtained from autocorrelation measurements at the sample position. In order to prevent any sample degradation and thermal grating contributions to the signal, the pulse energy was kept at less than 5 nJ/pulse. Both pump and probe beams were attenuated until the early-time signal shape was independent of pulse energy. To ensure that the samples were not photodegrading, the absorption spectrum of each sample was measured before and after the 3-TG scans.

V. EXPERIMENTAL RESULTS

The rotational averaging factors collected in Table 2 of Ref. 71 provide a means of testing the theory experimentally by examining different polarization sequences. That is only possible for heterodyne-detected 3-TG data, since then the sign of the signal can be resolved. For the polarization sequence VVVV we have $C_{1,3}^{(4)} = C_{2,4}^{(4)} = \frac{1}{5}$, for VVHH $C_{1,3}^{(4)} = C_{2,4}^{(4)} = \frac{2}{15}$. That is, the signals that reflect exciton population relaxation and recombination are always positive signed. For VHVH we find $C_{1,3}^{(4)} = \frac{2}{15}$ while $C_{2,4}^{(4)} = -\frac{2}{15}$. Thus the VHVH signal is positive signed, and its intensity diminishes as exciton spin relaxation increases the proportion of polarization radiated as $P_2^{(3)}$ and $P_4^{(3)}$. On the other hand, for VHHV we obtain $C_{1,3}^{(4)} = -\frac{2}{15}$ and $C_{2,4}^{(4)} = \frac{2}{15}$. That is, this signal is uniquely negative in sign, and its magnitude decreases with spin relaxation. Hence the theory for these experiments may be verified by measuring the sign of the 3-TG signals, which

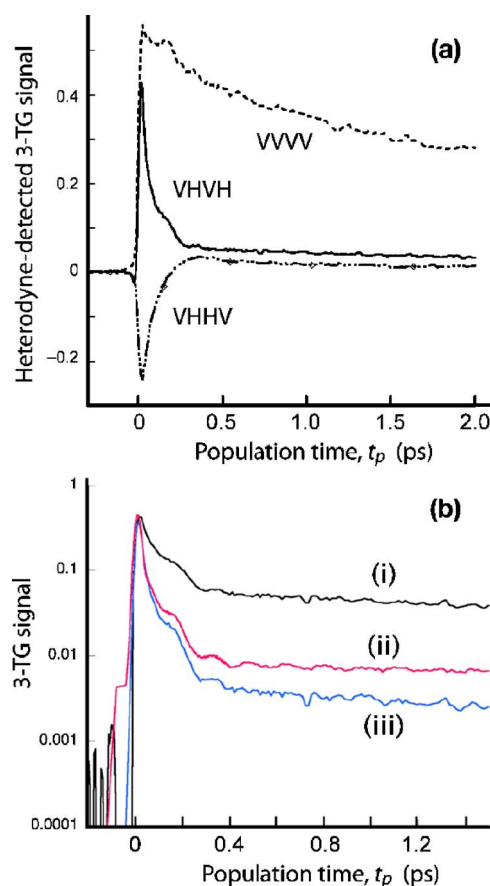


FIG. 7. (Color online) (a) Imaginary part of the heterodyne-detected 3-TG signals for CdSe quantum dots with average radius $R=1.72$ nm. The VVVV, VHVH, and VHHV signals are compared. The intensity scale for this plot is linear. (b) Comparison of (i) the VHVH signal for the $R=1.72$ nm CdSe sample shown in (a) with (ii) the homodyne-detected VHVH 3-TG data for CdSe with $R=1.70$ nm. Curve (iii) is the homodyne signal reconstructed from the real and imaginary parts of the heterodyne-detected 3-TG data, which is evidently qualitatively similar to curve (ii).

should always be positive except for VHHV. The corresponding experimental results are shown in Fig. 7(a). It is also seen in the figure that the VHHV signal acquires a positive sign after ~ 300 fs. That is because some QDs are excited to the $F=0$ states, as discussed in a future report. Note that in the present paper we report only the imaginary, that is, the absorptive, 3-TG signals.

In Fig. 7(b) the heterodyne-detected 3-TG data collected for CdSe quantum dots with average radius $R=1.72$ nm at 293 K in toluene solution are compared to homodyne-detected data for CdSe QDs with $R=1.70$ nm at 293 K in a poly(methylmethacrylate) polymer film. The latter data were reported in Ref. 72. Comparable data to the homodyne detected measurement are reconstructed from the real and imaginary parts of the heterodyne-detected data by taking the appropriate modulus squared.

In Fig. 8 we show the results of a control experiment—the heterodyne-detected data analogous to the homodyne-detected control experiment reported in the supporting information for Ref. 72. 3-TG traces were recorded for a dilute

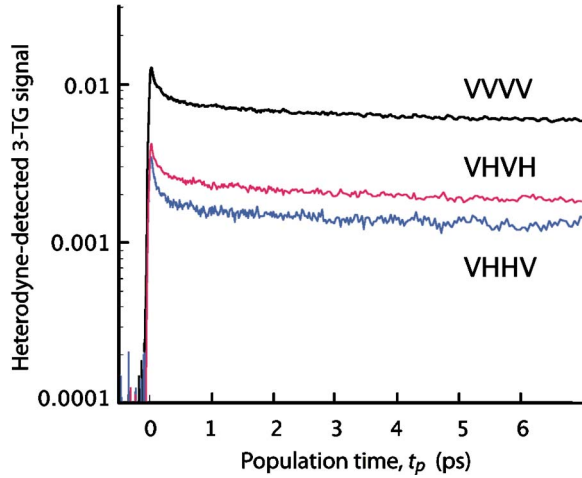


FIG. 8. (Color online) Results of a control experiment showing the heterodyne-detected 3-TG signals for VVVV, VHVH, and VHHV polarization sequences. These signals all contain the same information for this laser dye (rhodamine 6G) because its excited states obey selection rules for linearly-polarized light.

solution of the dye rhodamine 6G in ethanol. Like most molecules, rhodamine 6G has a simple dipolar transition moment oriented along an axis through the molecule. In that case the theory predicts that the only difference between the various polarization configurations should be an intensity factor. Indeed, that is what is observed in the comparison between 3-TG data recorded for the VVVV, VHVH, and VHHV polarization sequences, as shown in Fig. 8. It is noted that the change in sign of $C^{(4)}$ concomitant with an exciton spin flip is unique to QDs.

In order to extract the spin relaxation dynamics from the experimental VHVH (or VHHV) 3-TG data, account must be taken of the signal decay caused by population dynamics, as well as the spin relaxation contribution to the signal decay. The population dynamics are observed cleanly in the VVVV 3-TG data, so that information can be obtained independently from the cross-polarized 3-TG traces. If exciton recombination, which is very long compared to spin relaxation, were not complicated by fast surface trapping effects,^{102–105} then the VHVH data could be fit directly with an exponential function to retrieve the spin relaxation rate, as we employed in a previous report.⁷² A more accurate procedure that is well justified for the heterodyne-detected data, is to fit the cross-polarized 3-TG data with the function

$$I_{VHVH}(t_p) = [A_1 \exp(-2k_s t_p) + A_2] I_{VVVV}(t_p), \quad (21)$$

where $I_{VVVV}(t_p)$ is the decay profile of the VVVV 3-TG data as a function of pump-probe delay time t_p . The fitting procedure was undertaken for the data for CdSe quantum dots shown in Fig. 7(a). The VVVV signal was fit from $t_p \sim 100$ fs, thus avoiding the coherent spike, to three exponentials: one nanosecond component (too long to be resolved by our experiments) that represents exciton population relaxation, and two exponentials with relaxation rates of 0.28 and 2.2 ps^{-1} associated with surface trapping dynamics. The VHVH signal was then fit using Eq. (21), yielding an exciton

spin relaxation rate of 4.9 ps^{-1} ($\tau_s = 200$ fs). We have observed that these spin relaxation times rapidly lengthen as the QD size is increased.⁷²

In the theory section we explicitly described only the stimulated emission contribution to the 3-TG signals. The ground state recovery contribution follows the same temporal behavior, as is easily surmised. However, excited state absorption signals have an opposite sign to these former contributions to the signal. In other words, in a frequency dispersed pump-probe experiment there are two notable features: the negative changes in optical density, representing stimulated emission and ground state recovery of exciton populations, and the positive changes in optical density due to probe absorption into biexciton states.^{102,103} The effect of transient absorption signals on the 3-TG experiments with VVVV polarization sequences is to diminish the overall signal intensity. It might be expected that the implications for the VHVH and VHHV signals would be more problematic because measurement of exciton spin relaxation relies on sign changes, manifest through $C_1^{(4)}$ through $C_1^{(4)}$ (Table 1), in the induced polarizations. However, it turns out that while the polarizations radiated through signal pathways that involve probe absorption acquire a negative sign, as usual, the rotational average factors in the VHVH and VHHV signals also reverse sign.⁷¹ Hence the net effect is that the VHVH and VHHV signals are entirely unaffected by the relative proportion of ground state recovery, stimulated emission, and excited state absorption contributions to the signal.

VI. OPTICAL ORIENTATION USING CIRCULARLY-POLARIZED LIGHT

Circularly polarized (CP) light projects angular momentum onto the quantum dot exciton states. The result of that projection—whether the $F=+1$ or $F=-1$ exciton is photoexcited—depends on the handedness of the CP light, its propagation direction, and the orientation of the QD absorbing the photon. Colloidal QDs in an ensemble typically have no preferred orientation of their c axes in the laboratory frame axis system, so specific exciton states cannot be oriented by circularly polarized light. That is because the optical orientation is reversed when the QD is oppositely-facing relative to the propagation of the incident light. For example, Fig. 1 shows that the nominal selection rule for excitation of the Ψ_{-1} QD exciton involves using left-hand circularly polarized light. But, when the QD absorbs light from the opposite direction, then right-hand circularly polarized light excites the Ψ_{-1} exciton. However, the net projection of angular momentum onto the ensemble can be used to detect exciton relaxation. That can be achieved, for heterodyne detected measurements, by comparing the RRRR 3-TG signal intensity, where RRRR means the pump pulse pair, the probe, and the analyzer are right-circularly polarized, with corresponding RLL 3-TG data.

For a QD ensemble, where the QDs are each oriented randomly with respect to a fixed axis system, the difference intensity experiment can be understood through the rotational averaging approach reported previously.⁷¹ In this case, rather than the induced polarization changing sign (phase

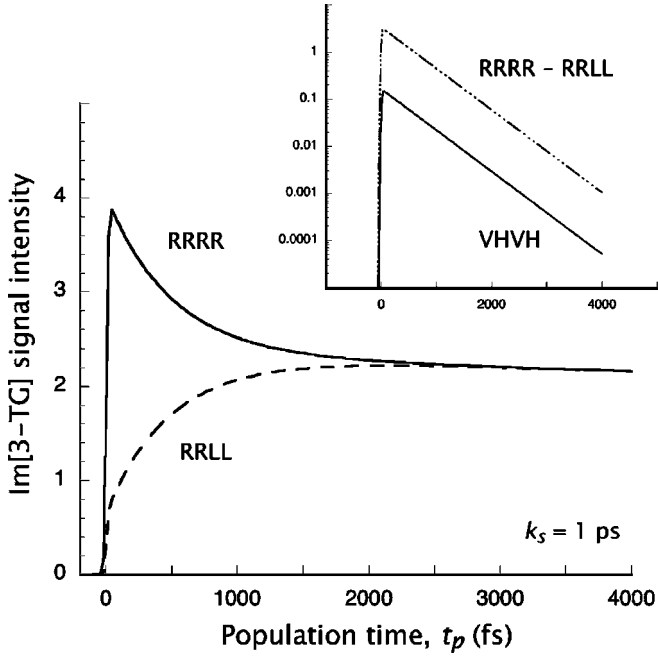


FIG. 9. Simulated RRRR and RRL 3-TG decays for a spin flip rate $k_s^{-1}=1$ ps. The inset compares the difference between the RRRR and RRL signal intensity to a comparable simulation of the VHVH 3-TG signal.

shifting) when population density flips spin state, it changes magnitude. For example, in the RRRR 3-TG signal, $C^{(4)}$ changes from $\frac{1}{5}$ to $\frac{1}{30}$. In the complementary experiment, RRL 3-TG, $C^{(4)}$ changes from $\frac{1}{30}$ to $\frac{1}{5}$. That can be more clearly seen in the four representative equations contributing to the total third-order polarization radiated in the RRRR 3-TG experiment

$$\mathbf{P}_1^{(3)}(0, t_p, t) = \frac{1}{5} |\boldsymbol{\mu}_{pg}|^4 \rho_1^{(3)}(0, t_p, t), \quad (22a)$$

$$\mathbf{P}_2^{(3)}(0, t_p, t) = \frac{1}{30} |\boldsymbol{\mu}_{pg}|^2 |\boldsymbol{\mu}_{mg}|^2 \rho_2^{(3)}(0, t_p, t), \quad (22b)$$

$$\mathbf{P}_3^{(3)}(0, t_p, t) = \frac{1}{5} |\boldsymbol{\mu}_{mg}|^4 \rho_3^{(3)}(0, t_p, t), \quad (22c)$$

$$\mathbf{P}_4^{(3)}(0, t_p, t) = \frac{1}{30} |\boldsymbol{\mu}_{mg}|^2 |\boldsymbol{\mu}_{pg}|^2 \rho_4^{(3)}(0, t_p, t). \quad (22d)$$

Simulations of the 3-TG experiments employing CP light obtained using Eqs. (22) and the corresponding equations for the RRL 3-TG experiment show clearly that the difference signal contains the same information as the VHVH and VHHV 3-TG experiments. Representative results of a calculation are shown in Fig. 9. Such an experiment can also be carried out using two pulses in a pump-probe configuration.³⁶ In practice, the difference measurement will have poor signal-to-noise compared to the direct measurement based on the linear polarization grating.

VII. DISCUSSION

Many semiconductors absorb light according to optical selection rules by which states can be selected by circularly

polarized light. The interesting aspect of such photoexcitation by circularly polarized light is that electrons are excited to defined spin states in the conduction band.²⁴ That, in turn, provides a route for defining the spin of electrons. We sought a means of using similar selection rules to investigate exciton fine structure in colloidal quantum dot ensembles; where the dots are oriented randomly with respect to the incident laser polarization. By using certain sequences of cross-linearly polarized light in a nonlinear optical experiment, we showed that the kinetics of exciton spin state flips can be measured directly in an isotropic ensemble of quantum dots.^{71,72} In the present work we examined that experiment further using simulations and a modified experimental set-up that uses heterodyne-detection of the third-order transient grating (3-TG) signal field.

For an oriented system the dynamics of exciton recombination versus spin relaxation can be probed using either circularly polarized light, or the crossed linear-polarized 3-TG experiment described here. Such experiments are relatively intuitive, and an elegant demonstration can be found reported in Ref. 34. For randomly oriented QDs, this clarity is lost. It was shown here that an understanding of the experimental data can only be grasped through a careful analysis of the appropriately averaged third-order response functions. In the present work we established a clear relationship between the VHVH/VHHV 3-TG polarization grating experiments and the difference measurement between the RRRR and RRL 3-TG signal intensities for the case when the signal field is heterodyne detected.

The simulations reported in Sec. III were dissected to reveal that the decay of the VHVH 3-TG signal does not correspond to diminishing radiated polarizations from sources in the ensemble; typically caused by population relaxation. The exciton spin flip is associated with a sign change $C^{(4)}$ that is manifest as a π phase shift of the induced polarizations $\mathbf{P}_2^{(3)}(0, t_p, t)$ and $\mathbf{P}_4^{(3)}(0, t_p, t)$, that emerge concomitant with spin relaxation, compared to $\mathbf{P}_1^{(3)}(0, t_p, t)$ and $\mathbf{P}_3^{(3)}(0, t_p, t)$. Hence the 3-TG signal decay is actually caused by destructive interference of the $\mathbf{P}_1^{(3)}(0, t_p, t)$ and $\mathbf{P}_3^{(3)}(0, t_p, t)$ polarizations with $\mathbf{P}_2^{(3)}(0, t_p, t)$ and $\mathbf{P}_4^{(3)}(0, t_p, t)$. To understand the way this works one needs to carry out the rotational averaging for the third-order spectroscopy. In doing so, each pathway from excitation to induced polarization needs to be separately considered to account for each transition dipole moment in the QD reference frame that interacts with the incident excitation pulses. That procedure emphasizes the coherent nature of the cross-polarized 3-TG spectroscopy, since the outcome of the experiment cannot be predicted by considering the independent action of the pump pulse pair and the probe.

The cross-polarized 3-TG experimental method we have described here measures spin relaxation among the QD $\Psi_{\pm 1}$ exciton states. We emphasize that the experiment measures bright exciton spin relaxation, not spin relaxation of dark excitons or electrons which can be detected in time-resolved Faraday rotation, for instance.^{35,36} Furthermore, all our experimental results were obtained at room temperature in the absence of an external magnetic field. It works because the transition dipole moments for these transitions are complex.

The precise means by which the exciton spin flip is promoted does not matter in terms of the success of the experiment, but systematic studies of size-, shape-, or material-dependent spin relaxation times may help to elucidate the mechanism. Possible mechanisms include the nonanalytic (long range) contribution to the electron-hole exchange interaction.^{57,62} Alternatively or additionally, spin-orbit coupling and exciton-phonon interactions can mediate a sequential electron and hole flip, via the dark exciton states for example.¹⁰⁶ Because of the rapid time-scale we find for exciton relaxation in CdSe QDs, possibilities such as spin randomization caused by trapping and detrapping of the electron in surface states are unlikely.

The experiments we have reported are for samples at 293 K, whereas most studies of QD fine structure are carried out at low temperatures, usually around 4 K, so that the homogenous line broadening is narrowed. When kT is much greater than the magnitude of the perturbation that mixes the $\Psi_{\pm 1}$ states, then electron-phonon coupling will tend to localize the exciton. In that case can we detect exciton spin relaxation using the cross-polarized 3-TG experiment. On the other hand, at low temperatures the interaction leads to mixed stationary states that would be observed in the frequency domain as a splitting of the $\Psi_{\pm 1}$ states. We reported here heterodyne-detected data for a CdSe QD and it was shown that those data can be used to reconstruct the homodyne-detected 3-TG data communicated by us recently.⁷² Results were also reported demonstrating that the sign of the 3-TG signal conforms to the sign dependence predicted by the theory.⁷¹ The initial sign of the VHVH 3-TG signal for QDs is positive, while that for the VHHV 3-TG signal is negative. Furthermore, control experiments on a model dye solution showed that for a linearly-polarized transition moment the 3-TG data show the same decay profile regardless of polarization sequence.

VIII. CONCLUSIONS

It was shown how cross linearly-polarized pulse sequences in three-pulse transient grating experiments form a polarization grating that monitors flipping among populations of quantum dot bright exciton spin states (those with total angular momentum $F=\pm 1$). Spin flips among those states lead to a decay of the grating, and consequently the diffracted probe signal. The experiment was simulated by solving the equations of motion that dictate the temporal evolution of the third-order density matrix. In the microscopic picture elucidated from the simulations, destructive interference between the third-order polarizations radiated by populations of excitons with flipped and conserved spin states causes the signal decay. Hence the signal provides a means to detect the history of the quantum dot exciton states. The results of experiments based on heterodyne detection of the radiated polarization that demonstrate and test the theory were reported. Those data, reported for a CdSe quantum dot sample, test the theory by confirming the sign dependence of the VHHV signal compared to VHVH and VVVV. It was found that exciton spin relaxation among the $F=\pm 1$ states occurs on a time scale of hundreds of femtoseconds, depend-

ing strongly on the quantum dot size. A control experiment on a laser dye in solution confirmed that the decay attributed to exciton spin relaxation is unique to quantum dots.

ACKNOWLEDGMENTS

The Natural Sciences and Engineering Research Council of Canada and the Alfred P. Sloan Foundation are gratefully acknowledged for support of this research. V. M. Huxter is thanked for valuable comments on the manuscript.

APPENDIX A: ORIENTATION DEPENDENCE OF QUANTUM DOT SPECTROSCOPY

In order to understand the rotational averaging and the nature of the transient grating experiment, it is useful to consider how the absorption of polarized light depends on the orientation of a QD. To that end we consider Eq. (A1), the matrix element for absorption, written in tensor form as

$$M_{\xi 0} \propto C = S_i T_i, \quad (\text{A1})$$

In general, the polarization vector of the incident radiation S_i is defined in a fixed (laboratory) axis system $i=x, y, z$, whereas the QD selection rules, Eqs. (8), refer to a local QD reference frame $\alpha=x', y', z'$. Those reference frames can be related via Euler transformation

$$C = S_i L_{i\alpha} T_\alpha, \quad (\text{A2})$$

where $L_{i\alpha}$ is the matrix of direction cosines. As the QD is rotated about the x' or y' axis by an angle $0 < \theta < \pi/2$ the Ψ_{+1} and Ψ_{-1} exciton states may both be excited to some extent by either RH or LH CP light because an elliptical polarization is projected onto the QD. In addition, the Ψ_0 exciton state may be excited. Consider excitation of the QD exciton states by RH CP light when the local QD axis system is oppositely oriented with respect to z , for example the QD is rotated by $\theta = \pi$ about x' or y' , as shown in Fig. 1. Then Eq. (A2) becomes, in matrix form

$$C = \begin{pmatrix} \hat{e}_x \\ i\hat{e}_y \\ 0 \end{pmatrix}^T \begin{pmatrix} 1 & 0 & 0 \\ 0 & -1 & 0 \\ 0 & 0 & -1 \end{pmatrix} \begin{pmatrix} \mu_{x'} \\ \mp i\mu_{y'} \\ 0 \end{pmatrix}, \quad (\text{A3})$$

where T indicates matrix transpose.

Recalling that the electric dipole transition moments for the $\Psi_{\pm 1}$ exciton states are $\boldsymbol{\mu}^{\pm 1} \propto (\mu_{x'}, \mp i\mu_{y'}, 0)$ it is evident that, upon rotation by π about either the x' or y' axes, the selection rules for optical orientation are reversed. In this case RH CP light excites the $\Psi_{-1}^{U,L}$ states exclusively, while LH CP light excites only the $\Psi_{+1}^{U,L}$ states. A diagram showing the change in selection rules for excitation of the $\Psi_{\pm 1}^{U,L}$ states is provided in Fig. 1. The implication of this result is that specific QD exciton states cannot be oriented by CP light if the ensemble is rotationally isotropic, such as colloidal samples. Nevertheless, a net angular momentum is projected onto the ensemble, which might be used to study the relaxation of free carrier spins.

The result stated above is consistent with the well-known concept from molecular spectroscopy that molecular transi-

tions cannot be photoselected from isotropic ensembles using absorption of polarized light. The origin of the reversed momentum projection when the CP light counterpropagates along the QD z' axis can be understood by considering the time-reversal symmetry of the interaction between CP light and the QD. Under time-reversal $\mathbf{k} \rightarrow -\mathbf{k}$, but the polarization of the CP light is unchanged (helices are chiral). That is analogous to exciting the QD with light propagating from the opposite z' direction. To consider how the electric dipole transition moment changes it is sufficient to consider how each of the single-excitation configuration wave functions changes. For instance, using spinor notation

$$\hat{T}\psi_{\uparrow,1/2} \propto \hat{T} \begin{pmatrix} s \\ u_{1/2} \end{pmatrix} = \begin{pmatrix} u_{1/2}^* \\ -s^* \end{pmatrix} = -i\psi_{\downarrow,-1/2}, \quad (\text{A4})$$

where \hat{T} is the time-reversal operator. It can thereby be deduced that, while RH CP light propagating such that $\mathbf{k} = \hat{z}'$ excites only exciton states with $F = +1$, when it propagates along the direction $\mathbf{k} = -\hat{z}'$, RH CP light excites only the $F = -1$ excitons.

APPENDIX B: SPECTROSCOPY OF ISOTROPIC QUANTUM DOT ENSEMBLES

Equation (A2) may be generalized to accommodate nonlinear spectroscopies of $(n-1)$ th order by taking $T_{\lambda_1, \dots, \lambda_n}$ to be a tensor of rank n denoting the QD response, in its local reference frame, to the action of n radiation-QD interactions.^{71,79–83} The latter interactions are described by S_{i_1, \dots, i_n} , where polarizations are defined in the fixed axis system. Thus

$$C^{(n)} = \langle S_{i_1, \dots, i_n} \ell_{i_1 \lambda_1} \cdots \ell_{i_n \lambda_n} T_{\lambda_1, \dots, \lambda_n} \rangle, \quad (\text{B1})$$

where $\ell_{i_j \lambda_j}$ are direction cosines and the angle brackets indicate that a rotational average will be taken.

Typically the tensor describing the QD response can be decomposed into a product of lower rank tensors. For example, for resonant $(n-1)$ th order nonlinear spectroscopies that tensor is written as a product of n electric dipole transition moments by using the factorization approximation.⁹⁸ In the present work a third-order spectroscopy is considered. A signal with wave vector $\mathbf{k}_s = -\mathbf{k}_1 + \mathbf{k}_2 + \mathbf{k}_3$ is induced to radiate from the sample and we can write $T_{\alpha\beta\gamma\delta} = \mu_{\alpha}^* \mu_{\beta} \mu_{\gamma} \mu_{\delta}^*$ for normal time-ordering of the radiation-matter interactions. In the case of a multilevel system the sequence of electric dipole transition moments is defined through a diagrammatic expansion of the induced polarization.^{96,97}

Rotational averaging of Eq. (B1) can be accomplished in a few different ways. Results for up to eighth rank tensors are known.⁸¹ Here the method of Andrews and Thirunamachandran⁷⁹ is applied. Each $\ell_{i_j \lambda_j}$ element in the product $\ell_{i_1 \lambda_1} \cdots \ell_{i_n \lambda_n}$ is an element in the Euler matrix, so Eq. (B1) can be written

$$C^{(n)} = S_{i_1, \dots, i_n} T_{\lambda_1, \dots, \lambda_n} I_{i_1, \dots, i_n; \lambda_1, \dots, \lambda_n}^{(n)}, \quad (\text{B2})$$

where

TABLE I. Rotational average weightings $C^{(4)}$, as defined in Eq. (B5). These are used, for example, in Eqs. (18)–(20) and (22). The values are taken from Ref. 71.

Polarization sequence	$C_1^{(4)}$	$C_2^{(4)}$	$C_3^{(4)}$	$C_4^{(4)}$
VVVV	$\frac{1}{5}$	$\frac{1}{5}$	$\frac{1}{5}$	$\frac{1}{5}$
VHVV	$\frac{2}{15}$	$-\frac{2}{15}$	$\frac{2}{15}$	$-\frac{2}{15}$
VHHV	$-\frac{2}{15}$	$\frac{2}{15}$	$-\frac{2}{15}$	$\frac{2}{15}$
RRRR	$\frac{1}{5}$	$\frac{1}{30}$	$\frac{1}{5}$	$\frac{1}{30}$
RRLL	$\frac{1}{30}$	$\frac{1}{5}$	$\frac{1}{30}$	$\frac{1}{5}$

$$I_{i_1, \dots, i_n; \lambda_1, \dots, \lambda_n}^{(n)} = \frac{1}{8\pi^2} \int_0^{2\pi} \int_0^{\pi} \int_0^{2\pi} \ell_{i_1 \lambda_1} \cdots \ell_{i_n \lambda_n} \sin \theta d\phi d\theta d\psi \quad (\text{B3})$$

and ϕ, θ, ψ are the Euler angles relating the fixed axis system to the local QD axis. As shown by Andrews and Thirunamachandran,⁷⁹ it is possible to express $I_{i_1, \dots, i_n; \lambda_1, \dots, \lambda_n}^{(n)}$ as a linear combination of isotropic tensors. In that case $N_n = n!/[2^{n/2}(n/2)!]$ isomers of each tensor must be considered (for even values of n). It can thereby be shown that $I_{i_1, \dots, i_n; \lambda_1, \dots, \lambda_n}^{(n)}$ may be written as a row vector of these isotropic tensors pertaining to the fixed axis system, times a matrix of coefficients, times a column vector of isotropic tensors relating to the local QD axis system. The isotropic tensors in the row and column vectors are products of $n/2$ Kronecker deltas. Hence for any third-order spectroscopy

$$I_{abcd; \alpha\beta\gamma\delta}^{(4)} = \frac{1}{30} \begin{pmatrix} \delta_{ab}\delta_{cd} \\ \delta_{ac}\delta_{bd} \\ \delta_{ad}\delta_{bc} \end{pmatrix}^T \begin{pmatrix} 4 & -1 & -1 \\ -1 & 4 & -1 \\ -1 & -1 & 4 \end{pmatrix} \begin{pmatrix} \delta_{\alpha\beta}\delta_{\gamma\delta} \\ \delta_{\alpha\gamma}\delta_{\beta\delta} \\ \delta_{\alpha\delta}\delta_{\beta\gamma} \end{pmatrix}. \quad (\text{B4})$$

By combining Eq. (B4) with Eq. (B2) and considering a signal in the $\mathbf{k}_s = -\mathbf{k}_1 + \mathbf{k}_2 + \mathbf{k}_3$ phase-matched direction, one obtains for a resonant spectroscopy

$$\begin{aligned} C^{(4)} &= \langle \epsilon_{\alpha}^{1*} \epsilon_{\beta}^2 \epsilon_{\gamma}^3 \epsilon_{\delta}^{4*} \rangle / (|\mu_{\alpha}| |\mu_{\beta}| |\mu_{\gamma}| |\mu_{\delta}|) \\ &= \frac{1}{30} \begin{pmatrix} (\hat{e}_{\alpha}^* \hat{e}_{\beta}) (\hat{e}_{\gamma} \hat{e}_{\delta}^*) \\ (\hat{e}_{\alpha}^* \hat{e}_{\gamma}) (\hat{e}_{\beta} \hat{e}_{\delta}^*) \\ (\hat{e}_{\alpha}^* \hat{e}_{\delta}) (\hat{e}_{\beta} \hat{e}_{\gamma}^*) \end{pmatrix}^T \begin{pmatrix} 4 & -1 & -1 \\ -1 & 4 & -1 \\ -1 & -1 & 4 \end{pmatrix} \\ &\quad \times \begin{pmatrix} (\hat{\mu}_{\alpha}^* \hat{\mu}_{\beta}) (\hat{\mu}_{\gamma} \hat{\mu}_{\delta}^*) \\ (\hat{\mu}_{\alpha}^* \hat{\mu}_{\gamma}) (\hat{\mu}_{\beta} \hat{\mu}_{\delta}^*) \\ (\hat{\mu}_{\alpha}^* \hat{\mu}_{\delta}) (\hat{\mu}_{\beta} \hat{\mu}_{\gamma}^*) \end{pmatrix}, \quad (\text{B5}) \end{aligned}$$

where the * indicates complex conjugate, as dictated by the phase-matching conditions. Laser pulses are labeled in order, $a-c$ and d labels the radiated polarization. Greek subscripts label the corresponding response of the QD in its reference frame. Values of $C^{(4)}$ determined for various polarization sequences discussed in this paper are collected in Table I.

- *Author to whom correspondence should be addressed. Electronic address: gscholes@chem.utoronto.ca
- ¹S. A. Wolf, D. D. Awschalom, R. A. Buhrman, J. M. Daughton, S. von Molnár, M. L. Roukes, A. Y. Chtchelkanova, and D. M. Treger, *Science* **294**, 1488 (2001).
 - ²H. Ohno, *Science* **281**, 951 (1998).
 - ³J. M. Kikkawa, I. P. Smorchkova, N. Samarth, and D. D. Awschalom, *Science* **277**, 1284 (1997).
 - ⁴J. Hubner, W. W. Ruhle, M. Klude, D. Hommel, R. D. R. Bhat, J. E. Sipe, and H. M. van Driel, *Phys. Rev. Lett.* **90**, 216601 (2003).
 - ⁵*Semiconductor Spintronics and Quantum Computation*, edited by D. D. Awschalom, N. Samarth, and D. Loss (Springer-Verlag, Berlin, 2002).
 - ⁶D. Loss and D. P. DiVincenzo, *Phys. Rev. A* **57**, 120 (1998).
 - ⁷A. Mizel and D. A. Lidar, *Phys. Rev. Lett.* **92**, 077903 (2004).
 - ⁸G. Burkard, H.-A. Engel, and D. Loss, *Fortschr. Phys.* **48**, 965 (2000).
 - ⁹I. Zutic, J. Fabian, and S. Das Sama, *Rev. Mod. Phys.* **76**, 323 (2004).
 - ¹⁰T. Calarco, A. Datta, P. Fedichev, E. Pazy, and P. Zoller, *Phys. Rev. A* **68**, 012310 (2003).
 - ¹¹S. Sangu, K. Kobayashi, A. Shojiguchi, and M. Ohtsu, *Phys. Rev. B* **69**, 115334 (2004).
 - ¹²B. W. Lovett, J. H. Reina, A. Nazir, B. Kothari, and G. A. Briggs, *Phys. Lett. A* **315**, 136 (2003).
 - ¹³D. D. Awschalom, *Physica E (Amsterdam)* **10**, 1 (2001).
 - ¹⁴H. Kamada and H. Gotoh, *Semicond. Sci. Technol.* **19**, S392 (2004).
 - ¹⁵D. K. Young, J. A. Gupta, E. Johnston-Halperin, Y. Kato, and D. D. Awschalom, *Semicond. Sci. Technol.* **17**, 275 (2002).
 - ¹⁶E. Pazy, E. Biolatti, T. Calarco, I. D'Amico, P. Zanardi, F. Rossi, and P. Zoller, *Europhys. Lett.* **62**, 175 (2003).
 - ¹⁷X. Li, Y. Wu, D. Steel, D. Gammon, T. H. Stievater, D. S. Katzer, D. Park, C. Piermarocchi, and L. J. Sham, *Science* **301**, 809 (2003).
 - ¹⁸D. Bimberg, M. Grundmann, and N. N. Ledentsov, *Quantum Dot Heterostructures* (Wiley, Chichester, 1999).
 - ¹⁹Al. L. Efros and A. L. Efros, *Sov. Phys. Semicond.* **16**, 772 (1982).
 - ²⁰L. E. Brus, *J. Chem. Phys.* **80**, 4403 (1984).
 - ²¹S. V. Gaponenko, *Optical Properties of Semiconductor Nanocrystals* (Cambridge University Press, Cambridge, 1998).
 - ²²L. Bányai and S. W. Koch, *Semiconductor Quantum Dots* (World Scientific, Singapore, 1993).
 - ²³A. P. Alivisatos, *J. Phys. Chem.* **100**, 13226 (1996).
 - ²⁴F. Meier and B. P. Zakharchenya, *Optical Orientation* (North Holland, Amsterdam, 1984).
 - ²⁵R. R. Parsons, *Phys. Rev. Lett.* **23**, 1152 (1969).
 - ²⁶E. F. Gross, A. I. Ekimov, B. S. Razbirin, and V. I. Safarov, *JETP Lett.* **14**, 70 (1971).
 - ²⁷C. Weisbuch and B. Vinter, *Quantum Semiconductor Structures: Fundamentals and Applications* (Academic, San Diego, 1991).
 - ²⁸R. I. Dzhioev, B. P. Zakharchenya, E. L. Ivchenko, V. L. Korenev, Yu. G. Kusraev, N. N. Ledentsov, V. M. Ustinov, A. E. Zhukov, and A. F. Tsatsul'nikov, *Phys. Solid State* **40**, 790 (1998).
 - ²⁹J. J. Baumberg, S. A. Crooker, D. D. Awschalom, N. Samarth, H. Luo, and J. K. Furdyna, *Phys. Rev. B* **50**, 7689 (1994).
 - ³⁰S. A. Crooker, D. D. Awschalom, J. J. Baumberg, F. Flack, and N. Samarth, *Phys. Rev. B* **56**, 7574 (1997).
 - ³¹C. Y. Hu, K. Morita, H. Sanada, S. Matsuzaka, Y. Ohno, and H. Ohno, *Phys. Rev. B* **72**, 121203(R) (2005).
 - ³²M. Z. Maialle, E. A. de Andrada e Silva, and L. J. Sham, *Phys. Rev. B* **47**, 15776 (1993).
 - ³³A. Vinattieri, J. Shah, T. C. Damen, D. S. Kim, L. N. Pfeiffer, M. Z. Maialle, and L. J. Sham, *Phys. Rev. B* **50**, 10868 (1994).
 - ³⁴O. Ikeuchi, S. Adachi, H. Sasakura, and S. Muto, *J. Appl. Phys.* **93**, 9634 (2003).
 - ³⁵J. A. Gupta, D. D. Awschalom, X. Peng, and A. P. Alivisatos, *Phys. Rev. B* **59**, R10421 (1999).
 - ³⁶J. A. Gupta, D. D. Awschalom, Al. L. Efros, and A. V. Rodina, *Phys. Rev. B* **66**, 125307 (2002).
 - ³⁷E. Tsitsishvili, R. v. Baltz, and H. Kalt, *Phys. Rev. B* **67**, 205330(R) (2003).
 - ³⁸M. Furis, J. A. Hollingsworth, V. I. Klimov, and S. A. Crooker, *J. Phys. Chem. B* **109**, 15332 (2005).
 - ³⁹R. I. Dzhioev, B. P. Zakharchenya, E. L. Ivchenko, V. L. Korenev, Yu. G. Kusraev, N. N. Ledentsov, V. M. Ustinov, A. E. Zhukov, and A. F. Tsatsul'nikov, *Phys. Solid State* **40**, 790 (1998).
 - ⁴⁰Yu. G. Kusrayev, A. V. Koudinov, B. P. Zakharchenya, S. Lee, J. K. Furdyna, and M. Dobrowolska, *Phys. Rev. B* **72**, 155301 (2005).
 - ⁴¹Al. L. Efros, *Phys. Rev. B* **46**, 7448 (1992).
 - ⁴²J.-B. Xia, *Phys. Rev. B* **40**, 8500 (1989).
 - ⁴³Al. L. Efros, M. Rosen, M. Kuno, M. Nirmal, D. J. Norris, and M. Bawendi, *Phys. Rev. B* **54**, 4843 (1996).
 - ⁴⁴M. Nirmal, D. J. Norris, M. Kuno, M. G. Bawendi, Al. L. Efros, and M. Rosen, *Phys. Rev. Lett.* **75**, 3728 (1995).
 - ⁴⁵E. Lifshitz, L. Fradkin, A. Glozman, and L. Langhof, *Annu. Rev. Phys. Chem.* **55**, 509 (2004).
 - ⁴⁶M. Chamarro, C. Gourdon, P. Lavallard, O. Lublinskaya, and A. I. Ekimov, *Phys. Rev. B* **53**, 1336 (1996).
 - ⁴⁷M. Furis, T. Barrick, P. Robbins, and S. A. Crooker, *Int. J. Mod. Phys. B* **18**, 3769 (2004).
 - ⁴⁸U. Woggon, F. Gindele, O. Wind, and C. Klingshirn, *Phys. Rev. B* **54**, 1506 (1996).
 - ⁴⁹R. T. Phillips, A. G. Steffan, S. R. Newton, T. L. Reinecke, and R. Kotlyar, *Phys. Status Solidi B* **238**, 601 (2003).
 - ⁵⁰Y. Chen, B. Gil, P. Lefebvre, and H. Mathieu, *Phys. Rev. B* **37**, 6429 (1988).
 - ⁵¹O. Gogolin, G. Mshvelidze, E. Tsitsishvili, R. Djanelidze, and C. Klingshirn, *J. Lumin.* **102-103**, 414 (2003).
 - ⁵²M. Bayer *et al.*, *Phys. Rev. B* **65**, 195315 (2002).
 - ⁵³U. Banin, J. C. Lee, A. A. Guzelian, A. V. Kadavanich, and A. P. Alivisatos, *Superlattices Microstruct.* **22**, 559 (1997).
 - ⁵⁴A. Franceschetti, L. Wang, H. Fu, and A. Zunger, *Phys. Rev. B* **58**, R13367 (1998).
 - ⁵⁵A. Franceschetti and A. Zunger, *Phys. Rev. Lett.* **78**, 915 (1997).
 - ⁵⁶T. Takagahara, *J. Lumin.* **87-89**, 308 (2000).
 - ⁵⁷T. Takagahara, *Phys. Rev. B* **62**, 16840 (2000).
 - ⁵⁸T. Takagahara, *Phys. Rev. B* **47**, 4569 (1993).
 - ⁵⁹E. L. Ivchenko, *Phys. Status Solidi A* **164**, 487 (1997).
 - ⁶⁰S. V. Gupalov and E. L. Ivchenko, *Phys. Solid State* **42**, 1976 (2000).
 - ⁶¹S. V. Gupalov, E. L. Ivchenko, and A. V. Kavokin, *Superlattices Microstruct.* **23**, 1205 (1998).
 - ⁶²S. V. Gupalov and E. L. Ivchenko, *J. Cryst. Growth* **184-185**, 393 (1998).
 - ⁶³K. Leung and K. B. Whaley, *Phys. Rev. B* **56**, 7455 (1997).
 - ⁶⁴K. Leung, S. Pokrant, and K. B. Whaley, *Phys. Rev. B* **57**, 12291

- (1998).
- ⁶⁵A. S. Bracker *et al.*, Phys. Rev. Lett. **94**, 047402 (2005).
- ⁶⁶M. Paillard, X. Marie, P. Renucci, T. Amand, A. Jbeli, and J. M. Gérard, Phys. Rev. Lett. **86**, 1634 (2001).
- ⁶⁷T. Watanuki, S. Adachi, H. Sasakura, and S. Muto, Appl. Phys. Lett. **86**, 63114 (2005).
- ⁶⁸O. I. Micic, H. M. Cheong, H. Fu, A. Zunger, J. R. Sprague, A. Mascarenhas, and A. J. Nozik, J. Phys. Chem. B **101**, 4904 (1997).
- ⁶⁹G. L. Bir and G. E. Pikus, *Symmetry and Strain-Induced Effects in Semiconductors* (Wiley, New York, 1975).
- ⁷⁰K. Cho, Phys. Rev. B **14**, 4463 (1976).
- ⁷¹G. D. Scholes, J. Chem. Phys. **121**, 10104 (2004).
- ⁷²V. M. Huxter, V. Kovalevskij, and G. D. Scholes, J. Phys. Chem. B **109**, 20060 (2005).
- ⁷³G. Dresselhaus, Phys. Rev. **100**, 580 (1955).
- ⁷⁴D. S. Klinger, J. W. Lewis, and C. E. Randall, *Polarized Light in Optics and Spectroscopy* (Academic Press, San Diego, 1990).
- ⁷⁵R. C. Jones, J. Opt. Soc. Am. **38**, 681 (1948).
- ⁷⁶G. D. Scholes and G. Rumbles (unpublished).
- ⁷⁷P. C. Sercel and K. J. Vahala, Phys. Rev. B **42**, 3690 (1990).
- ⁷⁸D. P. Craig and T. Thirunamachandran, *Molecular Quantum Electrodynamics* (Dover, Mineola, New York, 1998).
- ⁷⁹D. L. Andrews and T. Thirunamachandran, J. Chem. Phys. **67**, 5026 (1977).
- ⁸⁰D. L. Andrews and N. P. Blake, J. Phys. A **22**, 49 (1989).
- ⁸¹D. L. Andrews and W. A. Ghoul, J. Phys. A **14**, 1281 (1981).
- ⁸²G. Wagnière, J. Chem. Phys. **76**, 473 (1982).
- ⁸³W. M. McClain, J. Chem. Phys. **57**, 2264 (1972).
- ⁸⁴M. D. Fayer, Annu. Rev. Phys. Chem. **33**, 63 (1982).
- ⁸⁵J. T. Fourkas and M. D. Fayer, Acc. Chem. Res. **25**, 227 (1992).
- ⁸⁶J. T. Fourkas, R. Trebino, and M. D. Fayer, J. Chem. Phys. **97**, 69 (1992).
- ⁸⁷H. J. Eichler, P. Günter, and D. W. Pohl, *Laser-Induced Dynamic Gratings* (Springer-Verlag, Berlin, 1986).
- ⁸⁸T. S. Rose, W. L. Wilson, G. Wäckerle, and M. D. Fayer, J. Phys. Chem. **91**, 1704 (1987).
- ⁸⁹Y. Kimura, Y. Yamamoto, and M. Terazima, J. Chem. Phys. **123**, 54513 (2005).
- ⁹⁰M. Terazima, M. Takezaki, S. Yamaguchi, and N. Hirota, J. Chem. Phys. **109**, 603 (1998).
- ⁹¹E. Vauthey, C. Hogemann, and X. Allonas, J. Phys. Chem. A **102**, 7362 (1998).
- ⁹²Q.-H. Xu, G. D. Scholes, M. Yang, and G. R. Fleming, J. Phys. Chem. A **103**, 10348 (1999).
- ⁹³Q.-H. Xu, Y.-Z. Ma, and G. R. Fleming, J. Phys. Chem. A **106**, 10755 (2002).
- ⁹⁴M. Walther, V. Raicu, J. P. Ogilvie, R. Phillips, R. Kluger, and R. J. D. Miller, J. Phys. Chem. B **109**, 20605 (2005).
- ⁹⁵J. P. Ogilvie, M. Plazanet, G. Dadusc, and R. J. D. Miller, J. Phys. Chem. B **106**, 10460 (2002).
- ⁹⁶Y. R. Shen, *The Principles of Nonlinear Optics* (Wiley, New York, 1984).
- ⁹⁷S. Mukamel, *Principles of Nonlinear Optical Spectroscopy* (Oxford University Press, New York, 1995).
- ⁹⁸S. Mukamel, Phys. Rev. A **28**, 3480 (1983).
- ⁹⁹M. R. Salvador, M. A. Hines, and G. D. Scholes, J. Chem. Phys. **118**, 8380 (2003).
- ¹⁰⁰G. D. Goodno, G. Dadusc, and R. J. D. Miller, J. Opt. Soc. Am. B **15**, 1791 (1998).
- ¹⁰¹Q. Xu, Y. Ma, and G. R. Fleming, Chem. Phys. Lett. **338**, 254 (2001).
- ¹⁰²V. I. Klimov, D. W. McBranch, C. A. Leatherdale, and M. G. Bawendi, Phys. Rev. B **60**, 13740 (1999).
- ¹⁰³R. J. Ellingson, J. L. Blackburn, J. Nedeljkovic, G. Rumbles, M. Jones, H. X. Fu, and A. J. Nozik, Phys. Rev. B **67**, 075308 (2003).
- ¹⁰⁴P. Guyot-Sionnest, B. Wehrenberg, and D. Yu, J. Chem. Phys. **123**, 74709 (2005).
- ¹⁰⁵M. Braun, C. Burda, M. Mohamed, and M. El-Sayed, Phys. Rev. B **64**, 035317 (2001).
- ¹⁰⁶E. Tsitsishvili, R. v. Baltz, and H. Kalt, Phys. Rev. B **72**, 155333 (2005).